Explicitly Stochastic Parameterization of Nonorographic Gravity-Wave Drag

Stephen D. Eckermann * ..

Space Science Division, Naval Research Laboratory, Washington, DC 20375

* *Corresponding author address:* Stephen Eckermann, Code 7646, Space Science Division, Naval Research Laboratory, 4555 Overlook Avenue SW, Washington, DC 20375.

E-mail: stephen.eckermann@nrl.navy.mil

Report Documentation Page

Form Approved
OMB No. 0704-0188

1. REPORT DATE	2. REPORT TYPE	3. DATES COVERED
2010		**00-00-2010 to 00-00-2010**

4. TITLE AND SUBTITLE	5a. CONTRACT NUMBER
Explicitly Stochastic Parameterization of Nonorographic Gravity-Wave Drag	5b. GRANT NUMBER
	5c. PROGRAM ELEMENT NUMBER
6. AUTHOR(S)	5d. PROJECT NUMBER
	5e. TASK NUMBER
	5f. WORK UNIT NUMBER
7. PERFORMING ORGANIZATION NAME(S) AND ADDRESS(ES) **Naval Research Laboratory,Space Science Division,4555 Overlook Avenue SW,Washington,DC,20375**	8. PERFORMING ORGANIZATION REPORT NUMBER
9. SPONSORING/MONITORING AGENCY NAME(S) AND ADDRESS(ES)	10. SPONSOR/MONITOR'S ACRONYM(S)
	11. SPONSOR/MONITOR'S REPORT NUMBER(S)

12. DISTRIBUTION/AVAILABILITY STATEMENT
Approved for public release; distribution unlimited

13. SUPPLEMENTARY NOTES
Journal Atmospheric Sciences, submitted

14. ABSTRACT

We present a straightforward methodology for converting the deterministic multi-wave parameterizations of nonorographic gravity-wave drag, currently used in general circulation models (GCMs), to stochastic analogues that use far fewer waves (in our example, a single wave) within each grid box. Deterministic discretizations of source-level momentum flux spectra using a fixed spectrum of many waves with predefined phase speeds are replaced by sampling these source spectra stochastically using waves with randomly-assigned phase speeds. Using simple conversion formulas, we show that time-mean wave-induced drag diffusion and heating-rate profiles identical to those from the deterministic scheme are pro- duced by the stochastic analogue. Furthermore, the need for bulk intermittency factors of small value is largely obviated through the explicit incorporation of stochastic intermittency into the scheme. When implemented in a GCM, the single-wave stochastic analogue of an existing deterministic scheme reproduces almost identical time-mean middle-atmosphere climate and drag as its deterministic antecedent, but with an order of magnitude reduc- tion in computational expense. The stochastic parameterization is accompanied by natural stochastic variability about the time-mean profile that forces the smallest space-time scales of the GCM. Studies of mean GCM kinetic energy spectra show that this additional stochas- tic forcing does not lead to unrealistic increases in dynamical variability at these smallest GCM scales, although a systematic increase in divergent kinetic energy variability is evident. Our results show that the expensive deterministic schemes currently used in GCMs are easily modified and replaced by cheap stochastic analogues without any obvious deliterious impacts on GCM climate or variability, while offering potential advantages of computational savings reduction of systematic climate biases and greater and more realistic ensemble spread.

15. SUBJECT TERMS

16. SECURITY CLASSIFICATION OF:			17. LIMITATION OF ABSTRACT	18. NUMBER OF PAGES	19a. NAME OF RESPONSIBLE PERSON
a. REPORT **unclassified**	b. ABSTRACT **unclassified**	c. THIS PAGE **unclassified**	**Same as Report (SAR)**	**49**	

Standard Form 298 (Rev. 8-98)
Prescribed by ANSI Std Z39-18

ABSTRACT

We present a straightforward methodology for converting the deterministic multi-wave parameterizations of nonorographic gravity-wave drag, currently used in general circulation models (GCMs), to stochastic analogues that use far fewer waves (in our example, a single wave) within each grid box. Deterministic discretizations of source-level momentum flux spectra using a fixed spectrum of many waves with predefined phase speeds are replaced by sampling these source spectra stochastically using waves with randomly-assigned phase speeds. Using simple conversion formulas, we show that time-mean wave-induced drag, diffusion and heating-rate profiles identical to those from the deterministic scheme are produced by the stochastic analogue. Furthermore, the need for bulk intermittency factors of small value is largely obviated through the explicit incorporation of stochastic intermittency into the scheme. When implemented in a GCM, the single-wave stochastic analogue of an existing deterministic scheme reproduces almost identical time-mean middle-atmosphere climate and drag as its deterministic antecedent, but with an order of magnitude reduction in computational expense. The stochastic parameterization is accompanied by natural stochastic variability about the time-mean profile that forces the smallest space-time scales of the GCM. Studies of mean GCM kinetic energy spectra show that this additional stochastic forcing does not lead to unrealistic increases in dynamical variability at these smallest GCM scales, although a systematic increase in divergent kinetic energy variability is evident. Our results show that the expensive deterministic schemes currently used in GCMs are easily modified and replaced by cheap stochastic analogues without any obvious deliterious impacts on GCM climate or variability, while offering potential advantages of computational savings, reduction of systematic climate biases and greater and more realistic ensemble spread.

1. Introduction

Finite computational resources force global weather and climate prediction models to run at spatial resolutions that do not resolve the full spectrum of gravity waves that can exist in the atmosphere. Since the dissipation of gravity-wave momentum and energy induce significant body forces, heating and constituent mixing at synoptic scales, general circulation models (GCMs) must parameterize these missing gravity-wave-induced effects on the resolved flow (Kim et al. 2003). Parameterizations of drag due to unresolved orographic gravity waves were first implemented in weather and climate models over two decades ago, where they had immediate positive influences in the winter extratropical troposphere and stratosphere (Palmer et al. 1986; McFarlane 1987). They are now essential components of any credible global weather or climate prediction system.

Parameterizations of gravity waves from nonorographic sources were longer in coming, despite emerging understanding of their primary role in controlling the large-scale circulation of the middle atmosphere, particularly in the tropics and summer extratropics (Lindzen and Holton 1968; Dunkerton 1982b; Holton 1983; Garcia and Solomon 1985). Development was stymied at first by insufficient observational and theoretical knowledge of relevant nonorographic wave sources. High-resolution observations of gravity wave-induced velocity and temperature perturbations later revealed a broad spectrum of waves throughout the troposphere and middle atmosphere with surprisingly reproducible spectral shapes (Smith et al. 1987), which motivated an initial generation of nonorographic gravity wave drag parameterizations based on a quasi-invariant global background spectrum of many waves from indistinct tropospheric sources (e.g., Fritts and VanZandt 1993; Warner and McIntyre 1996).

A variety of these spectral nonorographic gravity-wave drag schemes now exist (e.g., Kiehl et al. 1996; Alexander and Dunkerton 1999; Medvedev and Klaassen 2000; Garcia et al. 2007) and they constitute the standard means of parameterizing nonorographic gravity wave drag in global models at present (see, e.g., Table 1 of Eyring et al. 2006). A next generation of schemes is slowly emerging, based on physical models of gravity-wave generation from specific nonorographic sources such as deep convection and frontogenesis: they too launch a broad spectrum of gravity waves (e.g., Charron and Manzini 2002; Song and Chun 2005) and can thus often be implemented by simply replacing the uniform source-level momentum flux function of a pre-existing spectral nonorographic scheme (e.g., Beres et al. 2005; Richter et al. 2010).

These parameterizations of nonorographic gravity-wave drag typically specify source-level wave momentum flux as a function of ground-based horizontal phase speed c, denoted $\tau_{src}(c)$, which is then discretized among n_{gw} individual gravity waves of phase speed c_j and momentum flux τ_j, where $j = 1 \ldots n_{gw}$. After assigning the remaining parameters of each tagged wave j (e.g., horizontal wavenumber vectors $\mathbf{K}_j$), the propagation and dissipation modules then determine how each wave's momentum flux is deposited into higher model levels. The resulting tendencies due to all the waves are summed and then applied to modify model winds and temperatures.

These $\tau_{src}(c)$ functions are typically broad, so that a large number of waves n_{gw} is often required for a sufficiently accurate discretization. Thus, unlike orographic gravity wave parameterizations that typically launch only 1 or 2 waves in each model grid box (Scinocca and McFarlane 2000; Webster et al. 2003), nonorographic schemes can launch anywhere from n_{gw} ∼10–1000 parameterized waves (Alexander and Dunkerton 1999; Scinocca 2003; Garcia

et al. 2007; Zhu et al. 2010; Orr et al. 2010). Consequently, nonorographic gravity wave drag parameterizations can be computationally expensive, which has spurred recent efforts to speed up specific schemes to make practical their integration into general circulation models (GCMs) used for production runs (e.g., Warner and McIntyre 2001; Scinocca 2003). This generally involves a set of simplifications or optimizations specific to that particular parameterization that do not change the underlying algorithm or output in any major way.

Here we investigate a different approach to this issue that is potentially applicable to any existing multiwave parameterization of nonorographic gravity-wave drag. The central idea is to replace the deterministic discretizations of $\tau_{src}(c)$ into n_{gw} individual waves with a stochastic discretization that can involve just a single parameterized wave in each model grid box. The approach is developed mathematically in application to a specific multiwave parameterization of nonorographic gravity-wave drag described in section 2. The stochastic analogue is described in section 3 and compared to its deterministic parent in single-column tests in section 4. The two are implemented in a GCM in section 5 and the GCM climate and variability that result from each in long-term integrations are compared and contrasted. The results are discussed in section 6 and the major findings and implications summarized in section 7.

2. Deterministic Parameterization

While the ideas to follow are general, we illustrate and implement them here for one specific scheme: the multiwave parameterization of nonorographic gravity wave drag implemented in version 3.0 of the Whole Atmosphere Community Climate Model (WACCM), as

summarized in Appendix A of Garcia et al. (2007). Full details of the scheme's formulation and numerics are provided by Kiehl et al. (1996), Collins et al. (2004) and Garcia et al. (2007), while Appendix A outlines the recent generalization of this parameterization code into a "team scheme" for use in GCMs at various US institutions. Here we discuss only those aspects of the scheme salient to the present work.

The scheme's prescribed source-level momentum flux function takes the Gaussian form

$$\tau_{src}(c) = \tau_b \exp\left[\frac{-(c-c_{off})^2}{c_w^2}\right], \quad (1)$$

$$\tau_b = \tau_b^* F(\phi, t), \quad (2)$$

with a phase-speed width $c_w = 30$ m s^{-1}. τ_b is the "background" momentum flux and is scaled from the constant baseline value τ_b^* by a factor $F(\phi, t)$, which varies with latitude ϕ and time (season) t, as given by eqs. (A24)–(A26) of Garcia et al. (2007) and plotted in Figure 1a.

This source flux $\tau_{src}(c)$ is discretized at the launch pressure level $p_{src} = 500$ hPa by assigning an equispaced distribution of ground-based horizontal phase speeds

$$c_j = c_{off} + j_* \Delta c, \quad (3)$$

$$j_* = -n_c, -n_c+1, \ldots + n_c - 1, +n_c = j - n_c + 1, (j_* \in \mathbf{Z}, n_c \in \mathbf{N}),$$

where Δc is the phase speed resolution, yielding a total of $n_{gw} = 2n_c + 1$ individual gravity waves of momentum flux $\tau_{src}(c_j)$. This phase speed distribution is symmetric about c_{off} and thus samples (1) symmetrically about it's peak.

In the Garcia et al. (2007) formulation, $c_{off} = U_{src} = |\mathbf{U}_{src}|$, where $\mathbf{U}_{src}$ is the horizontal velocity vector at p_{src}. Horizontal wavenumber vectors $\mathbf{K}_j$ align parallel to $\mathbf{U}_{src}$, yielding

a symmetric distribution of intrinsic horizontal phase speeds with flux peaking near zero intrinsic phase speed. Garcia et al. (2007) assign $n_{gw} = 65$ waves with $\Delta c = 2.5$ m s^{-1}, which yields intrinsic phase speeds spanning the range ± 80 m s^{-1}. The resulting discretized sampling of the normalized flux function $\tau_{src}(c)/\tau_b$ is plotted in black in Figure 2a. For comparison, the $n_{gw} = 9$, $\Delta c = 10$ m s^{-1} discretization used by Kiehl et al. (1996) is shown in gray, which, since they set $c_{off} = 0$, spans a ± 40 m s^{-1} range of ground-based phase speeds.

The subsequent deposition of wave momentum flux at higher altitudes is parameterized for each wave using a Lindzen (1981) parameterization of hydrostatic irrotational vertical propagation subject to critical-level removal and linear saturation thresholds (see Kiehl et al. 1996; Garcia et al. 2007, for details). The ensuing mean-flow acceleration $a_{j,k}$ (or gravity wave drag per unit mass) at model layer k due to wave j of phase speed c_j is

$$a_{j,k} = -g\epsilon \frac{\partial \tau_{j,k}}{\partial p}, \tag{4}$$

where g is gravitational acceleration, p is pressure, and ϵ is a constant in the range $0 < \epsilon \leq 1$ that represents the "intermittency" or "efficiency" of wave breaking. Intermittency factors of this sort appear in many multiwave nonorographic gravity-wave drag schemes but their implementation and effects can vary from scheme to scheme. The implementation here follows that in Alexander and Dunkerton (1999), and so, as in their scheme, if we retain the same ± 80 m s^{-1} range of phase speeds, then ϵ scales linearly with changes in Δc and inversely with the corresponding changes in n_{gw} to retain the same total mean-flow acceleration.

That total mean-flow acceleration

$$a_k^{tot} = \sum_{j=1}^{n_{gw}} a_{j,k}, \tag{5}$$

directed parallel to $\mathbf{U}_{src}$, is projected into zonal and meridional components that are applied as tendencies to the model's horizontal velocity field $\mathbf{U}_k$. The WACCM 3.0 scheme implements as options a number of additional limits on single-wave and total tendencies. These limits are applied in such a way that flux is redistributed rather than removed/added, so as to conserve column-integrated momentum. The version used here deposits all remaining wave flux in the top two model layers to ensure robust circulation and climate responses (Shaw et al. 2009).

With accelerations specified, other quantities follow based on the Lindzen (1981) saturation model. The effective vertical diffusion coefficient due to the turbulence generated by wave breaking is

$$\left(D_{gwd}\right)_k = \sum_{j=1}^{n_{gw}} \left[\left(\frac{Pr^{-1} |c_j - U_k^{proj}|}{2N_k^2} \right) a_{j,k} \right], \tag{6}$$

where U_k^{proj} is the component of the wind vector $\mathbf{U}_k$ projected along $\mathbf{K}_j$, N_k is buoyancy frequency in layer k, and Pr is the effective Prandtl number, here set equal to 4 following Garcia et al. (2007).

The wave-induced heating rate employed here is

$$\frac{\partial T_k}{\partial t} = \sum_{j=1}^{n_{gw}} \left\{ \frac{1}{C_p} \left(c_j - U_k^{proj} \right) a_{j,k} - \frac{T_k}{(1+Pr)} \frac{\partial}{\partial p} \left[\rho_k \left(c_j - U_k^{proj} \right) a_{j,k} \right] \right\}, \tag{7}$$

and is based on the work of Medvedev and Klaassen (2003), where T_k and ρ_k are temperature and density, respectively, in layer k and C_p is mass specific heat at constant pressure. The first term is a uniformly positive irreversible heating term due to deposition of total wave energy, both the frictional dissipation of wave kinetic energy and the thermal dissipation of wave potential energy. The second is a differential heating/cooling term associated with vertical variations in the wave heat flux, which Akmaev (2007) shows can only result from thermal

dissipation of wave potential energy, leading to the $1/(1+Pr)$ factor in (7). This heating rate expression is the only part of the parameterization used here that differs substantially from that described by Garcia et al. (2007).

3. Stochastic Analogue

Absent a specific nonorographic source model, the "background" flux function (1) is a practical choice that simplifies fitting of source parameters to observed climatological distributions of gravity-wave phase speeds and momentum fluxes (see, e.g., Alexander and Vincent 2000; Gong et al. 2008). To motivate what follows, however, a physical interpretation of it is useful here. For present purposes, one can view it as the state that emerges once a large number of random wave modes attain some form of statistical mechanical equilibrium (an analogy pursued explicitly in some spectral gravity-wave models: e.g., Allen and Joseph 1989; Souprayen et al. 2001). The equilibrium spectrum (1) would then emerge only over a volume and time both large and long enough, respectively, for the full ensemble of gravity-wave wavelengths and periods to attain equilibrium.

Given gravity-wave horizontal wavelengths of up to 1000 km and periods and group-propagation times of up to a day, typical GCM grid-box dimensions of 10-1000 km and time steps of 1-60 min would not appear to be either large or long enough, respectively, for this wave ensemble to equilibrate spectrally. Spectral equilibrium would appear instead only when averaged over wider horizontal areas encompassing many GCM grid boxes, and when averaged over a number of GCM time steps. At any given time step in one grid box, subgridscale wave flux would instead resemble the random nature of the component wave

modes themselves. Clearly, depending on model resolution, there is a continuum of possible states within a grid box, with the background multiwave "equilibrium" spectrum and a purely random stochastic state representing the two end limits.

A very simple approach to parameterizing such states is depicted in Figure 2b. Instead of discretizing (1) deterministically with n_{gw} equispaced wave phase speeds (Figure 2a), we now sample it randomly by choosing n_{sgw} "stochastic" waves with phase speeds

$$c_j = c_{off} + c_R \left(2R_j - 1\right), \tag{8}$$

where $j = 1 \ldots n_{sgw}$, $c_R = 80$ m s^{-1} is the phase speed range and R_j is the output from a random number generator with a uniform mean distribution, such that $0 \leq R_j \leq 1$. In this implementation, the random R_j values are repopulated at every grid point and at every model time step so that there are no spatiotemporal correlations in wave properties between adjacent grid boxes or model time steps, in contrast to the original deterministic scheme in which waves at adjacent grid boxes and times are highly correlated.

For a given bulk intermittency ϵ used in the original deterministic scheme, the same time mean momentum fluxes and total accelerations are attained in the stochastic analogue by using a scaled intermittency in (4) of

$$\epsilon_s = \epsilon \left(\frac{n_{gw}}{n_{sgw}} \right). \tag{9}$$

If ϵ parameterizes the bulk effects of stochastic intermittency alone in the deterministic scheme, one could argue such factors should be removed entirely from the stochastic analogue in which this intermittency is now explicit. Doing so is straightforward by adding a second uniformly distributed random variable S_j ($0 \leq S_j \leq 1$) and choosing a limit $\hat{S}$, such that if

$S_j \leq \hat{S}$ the stochastic acceleration a_k^{tot} is applied in the model, but if $S_j > \hat{S}$ we set $a_k^{tot} = 0$. Then ϵ_s disappears from (4), and is replaced by the new stochastic analogue of (9):

$$\hat{S} = \epsilon \left(\frac{n_{gw}}{n_{sgw}} \right). \tag{10}$$

Note that eqs. (9) and (10) can yield values in excess of unity. While $\epsilon_s > 1$ is technically unphysical the stochastic parameterization algorithm still works using such ϵ_s settings. By contrast $\hat{S} > 1$ cannot be accomodated, and so n_{sgw} needs to be increased until $\hat{S} < 1$ is achieved. Another way of viewing (10) is as a generalization of the stochastic scheme to a noninteger number of waves

$$\hat{n}_{sgw} = n_{sgw}\hat{S}. \tag{11}$$

This permits, for example, implementations with less than one stochastic wave per gridbox ($0 < \hat{n}_{sgw} < 1$), by choosing $n_{sgw} = 1$ and nonvanishing $\hat{S} < 1$. For simplicity, in this paper we only show results using the ϵ_s formulation, given the more straightforward connection to its deterministic antecedent.

4. Offline Single Column Tests

A convenient feature of the stochastic implementation in section 3 is the close connection that is maintained to the original deterministic scheme. The latter has been carefully refined and tuned for use in global models over many years. The simple relations in section 3 allow the core physics and tuned parameter settings of the determinstic scheme to translate to the stochastic analogue, which should in turn yield the same mean drag profiles. We demonstrate this here using offline single-column tests.

The top panels of Figure 3 show vertical profiles of instantaneous zonal and meridional winds at a grid point near the Alps after +12 hours of a T79L68 global model forecast initialized on 1 June 2007 at 0000 UTC. The model in question is the Advanced-Level Physics High-Altitude prototype of the Navy Operational Global Atmospheric Prediction System (NOGAPS-ALPHA), and the fields are part of the high-altitude forecast-assimilation runs described by Eckermann et al. (2009).

The forecast model in those runs used the deterministic WACCM 3.0 scheme to parameterize nonorographic gravity wave drag. Thus at this time and location the model passed these exact wind (and other meteorological) profiles to that parameterization, which in turn returned zonal and meridional mean-flow accelerations, vertical diffusivities and dynamical heating rates shown with thick solid gray curves in the remaining panels of Figure 3. Here we have used the same tuned parameter settings as in Eckermann et al. (2009), specifically $n_{gw} = 65$, $\Delta c = 2.5$ m s^{-1}, $p_{src} = 500$ hPa, $\tau_b^* = 1.75$ mPa and $\epsilon = 0.0175$.

Other curves in these lower four panels show results from our stochastic analogue of this scheme that uses only a single wave ($n_{sgw} = 1$). Here output from the stochastic parameterization was averaged over a number of separate calls ranging from 1 to 10000, using the same input wind profiles in every case, but with the random number R_j in (8) independently reinitialized during each call. The mean accelerations, diffusivities and heating rates after 1–10 calls in Figures 3c–3f are substantially different from the deterministic reference (gray curve) due to the random nature of the wave field. However, after 100 calls the mean profiles are quite similar to the reference curve, and after 1000–10000 calls the mean profiles overlay the deterministic reference curves. However, as shown in Figure 4, while the long-term means are the same, the stochastic version produces large standard deviations about that

mean, whereas, for the same input meteorological profiles, the original deterministic scheme has zero standard deviation.

Since $n_{sgw} = 1$ and $n_{gw} = 65$, from (9) we used a modified stochastic intermittency $\epsilon_s = 65\epsilon \sim 1.138$. Thus, by incorporating intermittency into the parameterization explicitly (Figure 4), the need for a parameterized bulk intermittency factor is now largely obviated. Of course the $\epsilon_s \sim 1$ result is specific to the tuned settings for this particular model configuration and thus probably fortuitous, with tuned values for other models likely leading to $\epsilon_s \neq 1$. Nonetheless, the trend away from very small ϵ values, implying highly intermittent or inefficient wave breaking, to values nearer unity through an explicit stochastic representation of intermittency in the parameterization, is clearly both a robust and physically self-consistent result.

One can reduce the large standard deviations in Figure 4 by increasing n_{sgw}. Figure 5 shows the corresponding mean zonal accelerations and standard deviations as n_{sgw} is progessively increased, with ϵ_s rescaled in each case as in (9). As n_{sgw} increases, the standard deviation reduces towards the vanishing deterministic limit. Thus $n_{sgw} > 1$ yields hybrid states that are a blend of the stochastic ($n_{sgw} = 1$) and deterministic ($n_{sgw} \to \infty$) limits.

5. Global Model Tests

Next we compare how the equivalent stochastic and determinstic versions of this nonorographic gravity-wave drag parameterization perform in a GCM. We use the forecast model component of NOGAPS-ALPHA with the same T79L68 formulation and physics settings described by Eckermann et al. (2009), except that here we:

- use a Webster et al. (2003) parameterization of orographic gravity-wave and flow-blocking drag instead of the Palmer et al. (1986) scheme.

- apply the nonorographic gravity wave-induced heating rate (7) to GCM temperature fields using $Pr = 4$.

The GCM is intialized on 1 June 2007 using the NOGAPS-ALPHA analysis fields described by Eckermann et al. (2009), then is integrated forward in time without assimilation update cycles to 1 January 2010. This "nature run" is constrained by 12 hourly analyzed sea- and land-surface temperatures, snow depths and ice concentrations at the lower boundary.

A series of these nature runs was performed initially to tune the nonorographic gravity-wave drag parameterization to yield a realistic zonal-mean middle atmosphere climate, which led to several changes from the default WACCM 3.0 settings described in earlier sections. First, the background flux τ_b in (2) was modified, as shown in Figure 1b, to center flux peaks closer to the solstices and to increase wave momentum fluxes at the equator. Second, we chose to launch nonorographic waves zonally rather than along the source-level wind direction. Third, we reduced the critical inverse Froude number for nonorographic gravity-wave breaking, Fr_c^{-1}, from 1 to 0.1, to force parameterized waves to break at lower altitudes, an approach often used to tune both orographic and nonorographic gravity-wave drag in GCMs (e.g., Norton and Thuburn 1999; Webster et al. 2003; Scinocca et al. 2008) and recently defended on theoretical grounds by Scinocca and Sutherland (2010).

Figure 6a shows 3-year average zonal-mean zonal winds for July from a control run without parameterized nonorographic gravity-wave drag, revealing unrealistically strong stratospheric jets that extend through the mesosphere. Figure 6b shows corresponding mean winds

from the nature run in which the deterministic nonorographic gravity-wave drag was activated using the tuned settings noted above, with $\tau_b^* = 10$ mPa, $\epsilon = 0.0375$ and $n_{gw} = 65$. These simulations with tuned nonorographic gravity-wave drag show more realistic stratospheric jets in both hemispheres, including better tilting of the winter (southern) jet and realistic reversal of the summer (northern) jet in the upper mesosphere.

Figure 6c shows results from the nature run using the stochastic analogue of the tuned deterministic nonorographic gravity-wave drag, using $n_{sgw} = 1$ and thus $\epsilon_s = 2.275$ according to (9). Visual comparison of Figures 6b and 6c reveals almost identical zonal wind structure, despite the imposition of explicitly stochastic, highly intermittent and "noisy" gravity-wave drag and heating rates in the latter GCM simulation. To verify this visual impression, Figure 6d plots the mean zonal wind difference fields between the stochastic and deterministic nature runs. Differences everywhere are small, particularly in the summer hemisphere.

Figure 7 plots the 3-year zonal-mean zonal mean-flow accelerations (top row) and heating rates (bottom row) for July due to parameterized nonorographic gravity-wave drag from the deterministic and stochastic nature runs. The time-mean accelerations and heating rates in the GCM again look largely identical. Small values of the difference fields, plotted on the right of Figure 7, again confirm that impression.

Since our offline single column simulations demonstrated that the stochastic approach gave identical time-mean accelerations and heating rates to its determinstic antecedent, these GCM results might not seem all that surprising. Yet in a fully interactive nonlinear GCM, it is not a given that highly intermittent stochastic drag will produce the same long-term GCM climate as it's smooth deterministic progenitor. Indeed, the corresponding two-year zonal-mean zonal winds in January, plotted in Figure 8, show that the winter (northern)

stratospheric zonal winds in this case are very different between the stochastic and deterministic nature runs. These differences arose due to spontaneous stratospheric warmings in both Januaries of the stochastic run which did not occur in the deterministic simulation: the latter generated a warming only in December 2007, which did not occur in the stochastic run. Of course, stratospheric warmings in northern winter are a well-known source of natural interannual variability in GCMs, and nature runs extending for 25-50 years or more would be needed to deduce any real systematic differences in zonal-mean northern winter stratospheric climate or stratospheric warming frequency due to use of stochastic or deterministic nonorographic gravity-wave drag (Charlton et al. 2007). Nonetheless, Figure 8 highlights the potential for the stochastic scheme to generate different GCM behavior than the deterministic version by more random forcing that can seed large irreversible changes via nonlinear interactions and feedbacks. The differences in the summer hemisphere in Figure 8b, which are also larger than those in the summer hemisphere in Figure 6d, are probably due to interhemispheric coupling through a modified mesospheric pole-to-pole residual circulation caused by modified gravity-wave driving in northern winter due to the differently disturbed winter stratospheres in each simulation (Becker and Fritts 2006).

Variability in the deterministic scheme's drag comes solely from variability in resolved GCM winds and temperatures, which in turn peaks at planetary wavenumbers. Thus, the deterministically parameterized nonorographic gravity-wave drag forces variability most strongly at the gravest GCM wavenumbers. By contrast, the stochastic scheme's drag also varies significantly and randomly from point to point in both space and time (Figure 4), and thus could force significant variability at the smallest space-time scales of the GCM. Since these smallest GCM scales can be unreliable and can alias to larger scales (Lander

and Hoskins 1997), such small-scale forcing might have undesirable side effects on the GCM simulations.

To investigate this, in each nature run the GCM's instantaneous global spectral fields were saved at 0000 UTC on every model day. Figure 9a plots mean total kinetic energy spectra at 0.055 hPa for June (2007-2009) for the stochastic and deterministic runs, along with the divergent and vortical contributions, as computed directly from these daily spherical harmonic spectral coefficients of GCM vorticity and divergence (e.g., Koshyk et al. 1999). In computing these long-term means, we also computed standard deviations at each total wavenumber, which are plotted in Figure 9b. In the row beneath, we plot the ratio of these spectral distributions between the GCM fields using stochastic and deterministic drag, for both the mean spectra (Figure 9c) and their standard deviations (Figure 9d). Overall, we do not see any noticeable change in either the shape or intensity of the mean GCM kinetic energy spectra between the stochastic and deterministic simulations. The only clear signal is in Figure 9d, which shows that the standard deviation of the divergent component of the GCM kinetic energy is systematically larger at the highest total wavenumbers in the simulation with stochastic gravity-wave drag.

To study these trends as a function of altitude, we averaged the spectral means and standard deviations at each height over the band of total wavenumbers 60–75 (shaded in Figure 9d). Figure 10 plots the height variation of the ratio of the mean spectra and their standard deviations between the stochastic and deterministic nature runs. Once again, the only clear trend with altitude is a slight overall increase in the standard deviation of divergent kinetic energy in the GCM at high total wavenumbers in the upper stratosphere and mesosphere when using the stochastic scheme, although mean divergent kinetic energy averaged

over height is also slightly higher systematically in Figure 10a. Why a similar enhancement in the standard deviation of small-scale GCM vorticity is not evident in Figure 10b is not clear. It may be that this stochastic gravity-wave forcing produces regional imbalances that lead to the rapid regeneration of secondary resolved gravity waves (divergent energy) in the GCM that propagate away to restore a balanced vorticity field (e.g., Vadas et al. 2003). In any event, these results indicate that highly stochastic and intermittent parameterizations of gravity-wave forcing, in addition to producing reliable GCM climate, do not appear to be accompanied by any major unrealistic increases in small-scale dynamical variability within the GCM.

6. Discussion

While there have been occasional efforts to parameterize nonorographic gravity-wave drag stochastically in GCMs (e.g., Dunkerton 1982a; Piani et al. 2004), the parameterizations currently used in production GCM configurations are exclusively multi-wave deterministic formulations. A strong practical motivation for the current stochastic approach to parameterizing nonorographic gravity-wave drag is to reduce the computational expense of these multi-wave deterministic schemes in GCMs. When the 65-wave WACCM 3.0 scheme of Garcia et al. (2007) was implemented in NOGAPS-ALPHA, for instance, it alone consumed between 20–35% of the forecast model's total run time. The extension of NOGAPS-ALPHA into the middle atmosphere involves additional model layers and physics that are slated for future transition to the operational NOGAPS. As a numerical weather prediction (NWP) prototype, new NOGAPS-ALPHA features compete for scarce computational resources with

many other potential upgrades to NOGAPS with potentially greater immediate impact on NWP (e.g., higher horizontal resolution, more tropospheric observations for assimilation, etc.). Thus, to be a viable candidate for near-term transition to operations, parameterizations of nonorographic gravity-wave drag must be both accurate and computationally cheap relative to the total run time of the system.

The single-wave stochastic analogue of the 65-wave scheme developed here should ideally yield close to a 65-fold increase in computational speed. As discussed in Appendix A, it was implemented here within the existing parameterization code, which contains significant additional overhead associated with internal calculations of different meteorological profiles and time-mean statistics, and thus a 65-fold speed increase cannot be expected. Nonetheless, without any additional effort to further optimize this parameterization subroutine, the single-wave stochastic option yields an order of magnitude increase in the speed of this subroutine relative to the deterministic 65-wave version in the NOGAPS-ALPHA nature runs reported here. The single-wave stochastic scheme now consumes between 1-4% of the forecast model's total run time and thus becomes a viable transition candidate. The computational expense issue is unique neither to this particular parameterization nor to this particular GCM. For example, in their implementation of the deterministic nonorographic gravity-wave drag scheme of Scinocca (2003) in the European Centre for Medium-Range Weather Forecasts Integrated Forecast System (ECMWF IFS), Orr et al. (2010) discretized their source momentum-flux spectrum using $n_{gw} = 80$ individual waves. Due to the resultant computational expense, they found it necessary to update the tendency from this scheme every two hours only, to reduce the overall computational burden to $\sim$3% of the total run time. Our stochastic approach allows us to achieve similar or greater computational savings

without resorting to a reduced space-time physics grid in the GCM.

A convenient aspect of the stochastic formulation developed here is the close relationship that is retained to the antecedent deterministic schemes, given that the latter schemes are now common in GCMs and have been exhaustively tuned over many years to yield realistic middle atmosphere climate. Using simple conversion relations, our offline single-column simulations showed that identical time-mean mean-flow accelerations, heating rates, and diffusivities could be generated using a straightforward stochastic analogue of a tuned determinisitic scheme. More importantly, when implemented within a GCM, nearly indistinguishable zonal-mean drag and zonal-mean climate were produced in July, for example. Such reproducible GCM climate responses were not assured given the potentially large nonlinear feedbacks involved in transitioning from drag that is smooth and deterministic, to drag that is noisy and random on small space-time scales. These findings essentially accord with those of McLandress and Scinocca (2005), who found that GCMs were remarkably insensitive to the precise ways in which nonorographic gravity-wave momentum fluxes were deposited as a function of height in different deterministic schemes.

The stochastic scheme produces random drag variability at the smallest space-time scales of the GCM that is entirely absent in the deterministic parent scheme. In essence, this variability now makes explicit in the GCM the inherent gravity-wave intermittency that is parameterized in the deterministic scheme using the bulk scaling factor ϵ. A body of literature has highlighted potential advantages of an explicit representation of such random intrinsic intermittency in GCM parameterizations (Palmer 2001; Palmer et al. 2005; Wilks 2008), such as more realistic ensemble spread and variability (Buizza et al. 1999, 2005; Teixeira and Reynolds 2008; Reynolds et al. 2008) and mean error reduction via more realistic

population of different climate and weather regimes (Molteni and Tibaldi 1990; Jung et al. 2005). Figure 8, for example, showed very different mean winter polar stratospheric winds in January between the stochastic and deterministic nature runs due to stratospheric warmings in the stochastic GCM simulation that did not occur in the deterministic simulation. These 2.5 year runs are far too short to deduce any systematic differences in stratospheric warming frequency. Nonetheless, these results are consistent with simple conceptual models that show how small amounts of random gravity wave forcing can trigger large regime transitions that generate stratospheric warmings that do not occur in a corresponding deterministic model without random gravity-wave forcing (Birner and Williams 2008).

Despite intense forcing at the smallest space-time scales of the GCM by the stochastic gravity-wave drag scheme, our GCM simulations did not reveal any large systematic increases in mean kinetic energy at the smallest GCM scales relative to the corresponding deterministic simulation, although a small systematic increase in the standard deviation of divergent kinetic energy at small resolved scales was clearly evident (Figure 9). This finding may explain why GCMs that numerically suppress realistic kinetic energy at small space-time scales see greatest improvements not via stochastic parameterization alone, but also by explicitly injecting additional stochastic kinetic energy back into these smallest resolved GCM scales (Jung et al. 2005; Berner et al. 2009; Charron et al. 2010).

Recent work has also found that mesoscale GCM kinetic energy in the mesosphere is intrinsically chaotic and stochastic due to the dominance of divergent gravity wave motions that have fast decorrelation times (Liu et al. 2009; Nezlin et al. 2009). Thus, the random stochastic forcing of the smallest mesospheric space-time scales of a GCM using a stochastic nonorographic gravity-wave drag parameterization may in fact mimic the true stochastic

nature of these dynamics in the GCM.

7. Conclusions

We have presented a simple methodology for generating an explicitly stochastic analogue of an existing deterministic multi-wave parameterization of nonorographic gravity-wave drag that should be easily applicable to other GCM parameterizations of gravity-wave drag. Our approach maintains a close association to the original deterministic scheme, such that the stochastic version is implemented here as an option and minor modification of the original deterministic parameterization code. Through the use of simple scaling terms, we show how the stochastic analogue reproduces identical time-mean drag, diffusion and heating rates to the deterministic parent scheme, which greatly simplifies replacing the latter with the former in GCMs using the existing tuned parameter settings of the deterministic antecedent.

When implemented in a GCM, our single-wave stochastic analogue of the 65-wave WACCM 3.0 deterministic nonorographic gravity-wave drag scheme produced largely identical zonal-mean climate and very similar spectral energy distributions in long-term nature runs to those from corresponding runs using the original deterministic scheme. In addition to reproducing very similar GCM climate and variability, the stochastic scheme yields the following additional beneficial features:

- an order-of-magntitude reduction in computational expense;
- explicit parameterization of gravity-wave intermittency, which largely replaces the tuned bulk intermittency factor ϵ in the deterministic scheme;

- stochastic GCM variability that can realistically increase ensemble spread and reduce mean climate biases.

Given these benefits along with no apparent disadvantages to date, we are now routinely parameterizing nonorographic gravity-wave drag in NOGAPS-ALPHA using the single-wave stochastic parameterization outlined here. Having made this change, new parameterization possibilities now open up. For example, there are emerging observations of gravity-wave momentum-flux intermittency (e.g., Hertzog et al. 2008), which could now be used to constrain the explicit stochastic variability of the parameterization more realistically (see, e.g., Figure 5). Similarly, there are other parameters in the scheme besides wave phase speeds that could be converted from deterministic to stochastic variables. Obvious candidates are those that are poorly constrained observationally or theoretically and which are likely to vary quasi-randomly rather than having set values, such as the background momentum flux τ_b^* and the launch pressure level p_{src}, among others.

A longer-term goal is to transition from the crude background sources used here to more physical parameterizations of nonorographic gravity-wave drag from specific tropospheric sources inferred from GCM fields, such as deep convection and jet instabilities (Charron and Manzini 2002; Beres et al. 2005; Richter et al. 2010). One might assume that physical source models would naturally lead back to a deterministic parameterization approach, but that may be unlikely. GCM parameterizations of convection remain challenging and are themselves moving towards explicitly stochastic models (Plant and Craig 2008; Teixeira and Reynolds 2008), which would naturally require a stochastic parameterization of the drag due to parameterized gravity waves emanating from such stochastic convective sources

in a GCM. Similarly, the jet instabilities and circulations that generate gravity waves are highly resolution dependent (e.g., Scinocca and Ford 2000; Plougonven and Snyder 2007). When these instabilities are properly resolved by the GCM, they likely generate resolved waves that do not need to be parameterized (e.g., O'Sullivan and Dunkerton 1995). Thus, the inadequately resolved nonorographic sources of unresolved gravity-wave momentum flux that require parameterization in GCMs may continue to be more usefully parameterized stochastically to reflect this inherent uncertainty and variability. Finally, it should be noted that aspects of orographic gravity-wave drag also appear to be inherently stochastic (Doyle and Reynolds 2008; Eckermann et al. 2010), which may motivate explicitly stochastic schemes to replace the deterministic parameterizations of orographic gravity-wave and flow-blocking drag that are currently used in GCMs (e.g., Palmer 2001).

Acknowledgments.

This research was supported by the Office of Naval Research through the NRL 6.1 work unit "Subgridscale Dynamics of Middle and Upper Atmospheres" and by NASA's Global Modeleing and Analysis Program, contract NNTG06HM19I. Discussions with Julio Bacmeister, In-Sun Song and Fabrizio Sassi on these topics are gratefully acknowledged.

APPENDIX A

Nonorographic Gravity Wave Drag Module

In 2006, NASA, NCAR and NRL began a collaborative project to develop gravity-wave-drag parameterization jointly for all three member GCMs: the Goddard Earth Observing System Version 5 (GEOS5), WACCM and NOGAPS-ALPHA, respectively. The scheme described by Kiehl et al. (1996) formed the basis for parameterized nonorographic gravity wave drag initially implemented within both WACCM and GEOS5. That common parameterization subsequently diverged. NCAR, *inter alia*, added more parameterized waves, used a wider phase-speed distribution and changed the source-level momentum flux for WACCM (Garcia et al. 2007). NASA adopted different source functions and modifed the propagation and dissipation modules for use in GEOS5. The Garcia et al. (2007) formulation in WACCM was later implemented in NOGAPS-ALPHA, where it too was modified and tuned for data assimilation applications (see section 3 of Eckermann et al. 2009). At the same time, the version in WACCM underwent further large independent changes (Richter et al. 2010).

It soon proved impossible for each center to continually integrate into its version of the code all the new features emerging at the other two centers, especially as the codes at each center became more dissimilar with time. This spurred a programming effort to combine the three different versions of the code at each center into a single common parameterization that all insititutions could then implement in their GCMs and develop jointly from a common code

and repository. This so-called "team scheme" was carefully coded from scratch to adhere rigidly to the 11 "plug compatibility" rules proposed by Kalnay et al. (1989) to facilitate easier exchange of parameterizations among modeling centers.

The biggest change relative to the antecedent codes was the creation of separate set-up and running subroutines (Rule 2), the former entirely new. This new set-up subroutine is called just once at the start of a GCM run. Through two simple input labels - a "model" and an "experiment" identifier - a series of specific statements and parameter settings are activated that define subsequent behavior of the gravity-wave-drag subroutine. The "model" label identifies a particular GCM by activating gravity-wave drag options and parameter values used in that GCM, and deactivating all other features used in other GCMs. The "experiment" label activates a secondary series of settings that activate preprogrammed "tuned" parameter values for a particular GCM experiment, configuration or resolution.

Given that the "team scheme" aims to be a community multi-institution GCM resource, the new set-up subroutine offers many advantages. For example:

- backwards compatibility: older code and/or tuned parameter settings can be retained and easily reactivated to rerun historical GCM experiments or configurations.

- faster transitions: new physics options developed for one center's GCM now become immediately available for other centers to activate and test in their GCM.

- greater flexibility: all physics options are available and can now be easily mixed and matched, or simply deactivated.

- separation of "tuning" from code development: casual GCM users seeking only to "tune" the parameterization in a GCM need only to make a few simple edits to the

set-up subroutine. The core physics subroutines of the parameterization should now never need to be edited by anyone other than parameterization developers.

While this integrated capability comes with an inevitable increase in the overall length and complexity of the code relative to it's antecedents, this is more than compensated for by these and other advantages.

Offline and online tests of the team scheme have verified exact reproduction of the results of the three antecedent nonorographic gravity-wave-drag codes previously run at NCAR, NASA and NRL, so that each center can now use the team scheme without any change in the tuned gravity-wave drag settings they have always used in their GCM. There is also no significant speed penalty of the new code relative to those antecdent codes in timing tests to date using the NOGAPS-ALPHA GCM.

This team scheme also integrates the different orographic gravity wave drag schemes used at each center, specifically: (a) an orographic gravity-wave scheme based on McFarlane (1987) used by NCAR and NASA (Kiehl et al. 1996), and (b) a Webster et al. (2003) parameterization of orographic gravity-wave and flow-blocking drag used in NOGAPS-ALPHA. In the team-scheme, source-level orographic gravity-wave fluxes from either scheme are sent to the same common propagation and dissipation modules used in the nonorographic gravity-wave calculations.

The stochastic parameterization of nonorographic gravity wave drag outlined in this paper has also been implemented in the team scheme as a new option, and was used to generate all the offline and online (GCM) results presented in this paper.

REFERENCES

Akmaev, R. A., 2007: On the energetics of mean-flow interactions with thermally dissipating gravity waves. *J. Geophys. Res.*, **112**, D11125, doi:10.1029/2006JD007908.

Alexander, M. J. and T. J. Dunkerton, 1999: A spectral parameterization of mean flow forcing due to breaking gravity waves. *J. Atmos. Sci.*, **56**, 4167–4182.

Alexander, M. J. and R. A. Vincent, 2000: Gravity waves in the tropical lower stratosphere: A model study of seasonal and interannual variability. *J. Geophys. Res.*, **105 (D14)**, 17,983–17,993.

Allen, K. R. and R. I. Joseph, 1989: A canonical statistical theory of oceanic internal waves. *J. Fluid Mech.*, **204**, 185–228.

Becker, E. and D. C. Fritts, 2006: Enhanced gravity-wave activity and interhemispheric coupling during the MaCWAVE/MIDAS northern summer program 2002. *Ann. Geophys.*, **24**, 1175–1188.

Beres, J. H., R. R. Garcia, B. A. Boville, and F. Sassi, 2005: Implementation of a gravity wave source spectrum parameterization dependent on the properties of convection in the Whole Atmosphere Community Climate Model (WACCM). *J. Geophys. Res.*, **110**, D10108, doi: 10.1029/2004JD005504.

Berner, J., G. J. Shutts, M. Leutbecher, and T. N. Palmer, 2009: A spectral stochastic

kinetic energy backscatter scheme and its impact on flow-dependent predictability in the ECMWF ensemble prediction system. *J. Atmos. Sci.*, **66**, 603–626.

Birner, T. and P. D. Williams, 2008: Sudden stratospheric warmings as noise-induced transitions. *J. Atmos. Sci.*, **65**, 3337–3343.

Buizza, R., P. L. Houtekamer, G. Pellerin, Z. Toth, Y. Zhu, and M. Wei, 2005: A comparison of the ECMWF, MSC, and NCEP global ensemble prediction systems. *Mon. Wea. Rev.*, **133**, 1076–1097.

Buizza, R., M. Miller, and T. N. Palmer, 1999: Stochastic representation of model uncertainties in the ECMWF ensemble prediction system. *Quart. J. Roy. Meteor. Soc.*, **125**, 2887–2908.

Charlton, A. J., et al., 2007: A new look at stratospheric sudden warmings. Part II: Evaluation of numerical model simulations. *J. Climate*, **20**, 470–488.

Charron, M. and E. Manzini, 2002: Gravity waves from fronts: Parameterization and middle atmosphere response in a general circulation model. *J. Atmos. Sci.*, **59**, 923–941.

Charron, M., G. Pellerin, L. Spacek, P. L. Houtekamer, N. Gagnon, H. L. Mitchell, and L. Michelin, 2010: Toward random sampling of model error in the Canadian ensemble prediction system. *Mon. Wea. Rev.*, **138**, 1877–1901.

Collins, W. D., et al., 2004: Description of the NCAR Community Atmosphere Model (CAM 3.0). NCAR Tech. Note NCAR/TN-464+STR, 214 pp. Http://www.ccsm.ucar.edu/models/atm-cam/.

Doyle, J. D. and C. A. Reynolds, 2008: Implications of regime transitions for mountain-wave-breaking predictability. *Mon. Wea. Rev.*, **136**, 5211–5223.

Dunkerton, T. J., 1982a: Stochastic parameterization of gravity wave stresses. *J. Atmos. Sci.*, **39**, 1711–1725.

Dunkerton, T. J., 1982b: Theory of the mesopause semiannual oscillation. *J. Atmos. Sci.*, **39**, 2681–2690.

Eckermann, S. D., J. Lindeman, D. Broutman, J. Ma, and Z. Boybeyi, 2010: Momentum fluxes of gravity waves generated by variable Froude number flow over three-dimensional obstacles. *J. Atmos. Sci.*, **67**, 2260–2278.

Eckermann, S. D., et al., 2009: High-altitude data assimilation system experiments for the northern summer mesosphere season of 2007. *J. Atmos. Sol.-Terr. Phys.*, **71**, 531–551.

Eyring, V., et al., 2006: Assessment of temperature, trace species, and ozone in chemistry-climate model simulations of the recent past. *J. Geophys. Res.*, **111**, D22308, doi:10.1029/2006JD007327.

Fritts, D. C. and T. E. VanZandt, 1993: Spectral estimates of gravity wave energy and momentum fluxes. Part i: Energy dissipation, acceleration, and constraints. *J. Atmos. Sci.*, **50**, 3685–3694.

Garcia, R. R., D. R. Marsh, D. E. Kinnison, B. A. Boville, and F. Sassi, 2007: Simulation of secular trends in the middle atmosphere, 1950–2003. *J. Geophys. Res.*, **112**, D09301, doi:10.1029/2006JD007485.

Garcia, R. R. and S. Solomon, 1985: The effect of breaking gravity waves on the dynamics and chemical composition of the mesosphere and lower thermosphere. *J. Geophys. Res.*, **90**, 3850–3868.

Gong, J., M. A. Geller, and L. Wang, 2008: Source spectra information derived from U.S. high-resolution radiosonde data. *J. Geophys. Res.*, **113**, D10106, doi:10.1029/2007JD009252.

Hertzog, A., G. Boccara, R. A. Vincent, F. Vial, and P. Cocquerez, 2008: Estimation of gravity wave momentum flux and phase speeds from quasi-Lagrangian stratospheric balloon flights. Part II: Results from the Vorcore campaign in Antarctica. *J. Atmos. Sci.*, **65**, 3056–3070.

Holton, J. R., 1983: The influence of gravity wave breaking on the general circulation of the middle atmosphere. *J. Atmos. Sci.*, **40**, 2497–2507.

Jung, T., T. N. Palmer, and G. J. Shutts, 2005: Influence of a stochastic parameterization on the frequency of occurrence of North Pacific weather regimes in the ECMWF model. *Geophys. Res. Lett.*, **32**, L23811, doi:10.1029/2005GL024248.

Kalnay, E., et al., 1989: Rules for the interchange of physical parameterizations. *Bull. Amer. Meteor. Soc.*, **70**, 620–622.

Kiehl, J. T., J. J. Hack, G. D. Bonan, B. A. Boville, B. P. Brieglab, D. L. Williamson, and P. J. Rasch, 1996: Description of the NCAR Community Climate Model (CCM3). NCAR Tech. Note NCAR/TN-420+STR, 152 pp. URL `http://www.cgd.ucar.edu/cms/ccm3/TN-420/`.

Kim, Y.-J., S. D. Eckermann, and H.-Y. Chun, 2003: An overview of the past, present, and future of gravity-wave drag parameterization for numerical climate and weather prediction models. *Atmos.-Ocean*, **41**, 65–98.

Koshyk, J. N., B. A. Boville, K. Hamilton, E. Manzini, and K. Shibata, 1999: Kinetic energy spectrum of horizontal motions in middle-atmosphere models. *J. Geophys. Res.*, **104**, 27 177–27 190.

Lander, J. and B. J. Hoskins, 1997: Believable scales and parameterizations in a spectral transform model. *Mon. Wea. Rev.*, **125**, 292–303.

Lindzen, R. S., 1981: Turbulence and stress owing to gravity wave and tidal breakdown. *J. Geophys. Res.*, **86**, 9707–9714.

Lindzen, R. S. and J. R. Holton, 1968: A theory of the quasi-biennial oscillation. *J. Atmos. Sci.*, **25**, 1095–1107.

Liu, H.-L., F. Sassi, and R. R. Garcia, 2009: Error growth in a whole atmosphere climate model. *J. Atmos. Sci.*, **66**, 173–186.

McFarlane, N. A., 1987: The effect of orographically excited gravity-wave drag on the general-circulation of the lower stratosphere and troposphere. *J. Atmos. Sci.*, **44**, 1775–1800.

McLandress, C. and J. F. Scinocca, 2005: The GCM response to current parameterizations of nonorographic gravity wave drag. *J. Atmos. Sci.*, **62**, 2394–2413.

Medvedev, A. S. and G. P. Klaassen, 2000: Parameterization of gravity wave momentum

deposition based on nonlinear wave interactions: Basic formulation and sensitivity tests. *J. Atmos. Sol.-Terr. Phys.*, **62**, 1015–1033.

Medvedev, A. S. and G. P. Klaassen, 2003: Thermal effects of saturating gravity waves in the atmosphere. *J. Geophys. Res.*, **108 (D2)**, 4040, doi:10.1029/2002JD002504.

Molteni, F. and S. Tibaldi, 1990: Regimes in the wintertime circulation over northern extratropics. II: Consequences for dynamical predictability. *Quart. J. Roy. Meteor. Soc.*, **116**, 1263–1288.

Nezlin, Y., Y. J. Rochon, S. Polavarapu, A. S. Medvedev, and G. P. Klaassen, 2009: Impact of tropospheric and stratospheric data assimilation on mesospheric prediction. *Tellus*, **61A**, 154–159.

Norton, W. A. and J. Thuburn, 1999: Sensitivity of mesospheric mean flow, planetary waves, and tides to strength of gravity wave drag. *J. Geophys. Res.*, **104**, 30 897–30 912.

Orr, A., P. Bechtold, J. Scinocca, M. Ern, and M. Janiskova, 2010: Improved middle atmosphere climate and forecasts in the ECMWF model through a non-orographic gravity wave drag parametrization. *J. Climate*, **in press**, doi:10.1175/2010JCLI3490.1, URL `http://journals.ametsoc.org/doi/abs/10.1175/2010JCLI3490.1`, `http://journals.ametsoc.org/doi/pdf/10.1175/2010JCLI3490.1`.

O'Sullivan, D. and T. J. Dunkerton, 1995: Generation of inertia-gravity waves in a simulated life cycle of baroclinic instability. *J. Atmos. Sci.*, **52**, 3695–3716.

Palmer, T. N., 2001: A nonlinear dynamical perspective on model error: A proposal for

non-local stochastic-dynamic parametrization in weather and climate prediction models. *Quart. J. Roy. Meteor. Soc.*, **127**, 279–304.

Palmer, T. N., G. J. Shutts, R. Hagedorn, F. J. Doblas-Reyes, T. Jung, and M. Leutbecher, 2005: Representing model uncertainty in weather and climate prediction. *Annu. Rev. Earth Planet. Sci.*, **33**, 163–193.

Palmer, T. N., G. J. Shutts, and R. Swinbank, 1986: Alleviation of a systematic westerly bias in general-circulation and numerical weather prediction models through an orographic gravity-wave drag parametrization. *Quart. J. Roy. Meteor. Soc.*, **112**, 1001–1039.

Piani, C., W. A. Norton, and D. A. Stainforth, 2004: Equatorial stratospheric response to variations in deterministic and stochastic gravity wave parameterizations. *J. Geophys. Res.*, **109**, D14101, doi:10.1029/2004JD004656.

Plant, R. S. and G. C. Craig, 2008: A stochastic parameterization for deep convection based on equilibrium statistics. *J. Atmos. Sci.*, **65**, 87–105.

Plougonven, R. and C. Snyder, 2007: Inertia-gravity waves spontaneously generated by jets and fronts. Part I: Different baroclinic life cycles. *J. Atmos. Sci.*, **64**, 2502–2520.

Reynolds, C. A., J. Teixeira, and J. D. McLay, 2008: Impact of stochastic convection on the ensemble transform. *Mon. Wea. Rev.*, **136**, 4517–4526.

Richter, J. H., F. Sassi, and R. R. Garcia, 2010: Towards a physically based gravity wave source parameterization in a general circulation model. *J. Atmos. Sci.*, **67**, 136–156.

Scinocca, J. F., 2003: An accurate spectral nonorographic gravity wave drag parameterization for general circulation models. *J. Atmos. Sci.*, **60**, 667–682.

Scinocca, J. F. and R. Ford, 2000: The nonlinear forcing of large-scale internal gravity waves by stratified shear instability. *J. Atmos. Sci.*, **57**, 653–672.

Scinocca, J. F. and N. A. McFarlane, 2000: The parameterization of drag induced by stratified flow over anisotropic orography. *Quart. J. Roy. Meteor. Soc.*, **126**, 2353–2393.

Scinocca, J. F., N. A. McFarlane, M. Lazare, J. Li, and D. Plummer, 2008: The CCCma third generation AGCM and its extension into the middle atmosphere. *Atmos. Chem. Phys.*, **8**, 7055–7074.

Scinocca, J. F. and B. R. Sutherland, 2010: Self-acceleration in the parameterization of orographic gravity wave drag. *J. Atmos. Sci.*, **67**, 2537–2546.

Shaw, T. A., M. Sigmond, T. G. Shepherd, and J. F. Scinocca, 2009: Sensitivity of simulated climate to conservation of momentum in gravity wave drag parameterization. *J. Climate*, **22**, 2726–2742.

Smith, S. A., D. C. Fritts, and T. E. VanZandt, 1987: Evidence for a saturated spectrum of atmospheric gravity waves. *J. Atmos. Sci.*, **44**, 1404–1410.

Song, I.-S. and H.-Y. Chun, 2005: Momentum flux spectrum of convectively forced internal gravity waves and its application to gravity wave drag parameterization. *J. Atmos. Sci.*, **62**, 107–124.

Souprayen, C., J. Vanneste, A. Hertzog, and A. Hauchecorne, 2001: Atmospheric gravity wave spectra: A stochastic approach. *J. Geophys. Res.*, **106**, 24 071–24 086.

Teixeira, J. and C. A. Reynolds, 2008: Stochastic nature of physical parameterizations in ensemble prediction: A stochastic convection approach. *Mon. Wea. Rev.*, **136**, 483–496.

Vadas, S. L., D. C. Fritts, and M. J. Alexander, 2003: Mechanism for the generation of secondary waves in wave breaking regions. *J. Atmos. Sci.*, **60**, 194–214.

Warner, C. D. and M. E. McIntyre, 1996: On the propagation and dissipation of gravity wave spectra through a realistic middle atmosphere. *J. Atmos. Sci.*, **53**, 3213–3235.

Warner, C. D. and M. E. McIntyre, 2001: An ultrasimple spectral parameterization for nonorographic gravity waves. *J. Atmos. Sci.*, **58**, 1837–1857.

Webster, S., A. R. Brown, D. R. Cameron, and C. P. Jones, 2003: Improvements to the representation of orography in the Met Office Unified Model. *Quart. J. Roy. Meteor. Soc.*, **129**, 1989–2010.

Wilks, D. S., 2008: Effects of stochastic parametrization on conceptual climate models. *Phil. Trans. R. Soc. A*, **366**, 2477–2490.

Zhu, X., J.-H. Yee, W. H. Swartz, E. R. Talaat, and L. Coy, 2010: A spectral parameterization of drag, eddy diffusion, and wave heating for a three-dimensional flow induced by breaking gravity waves. *J. Atmos. Sci.*, **67**, 2520–2536.

List of Figures

9 (a) mean kinetic energy spectra and (b) its standard deviation at each total wavenumber, at 0.055 hPa, averaged from daily 0000 UTC spectral NOGAPS-ALPHA GCM fields for June 2007-2009 for nature runs in which nonorographic gravity-wave drag was parameterized deterministically (gray curves) and stochastically (black curves). The vortical (dashed curves) and divergent (dotted curves) contributions to total kinetic energy (solid curves) are also shown. Panels below show the ratios of the stochastic to the deterministic spectral curves in the panels above. Panel (d) shades the total wavenumber range 60–75 used to form profile means in Figure 10. 47

10 Ratios of total (solid), divergent (dotted) and vortical (dashed) contributions to (a) mean kinetic energy and (b) its standard deviation in the NOGAPS-ALPHA GCM fields for June 2007–2009 using parameterized stochastic and deterministic nonorographic gravity-wave drag. Each energy value is averaged over the total wavenumber range 60–75, with the resulting ratios between the stochastic and deterministic GCM fields plotted as a function of height. Values greater (less) than unity imply increased (decreased) kinetic energy at wavenumbers 60–75 in the GCM fields with stochastic nonorographic gravity-wave drag, relative to those with deterministic nonorographic gravity-wave drag. 48

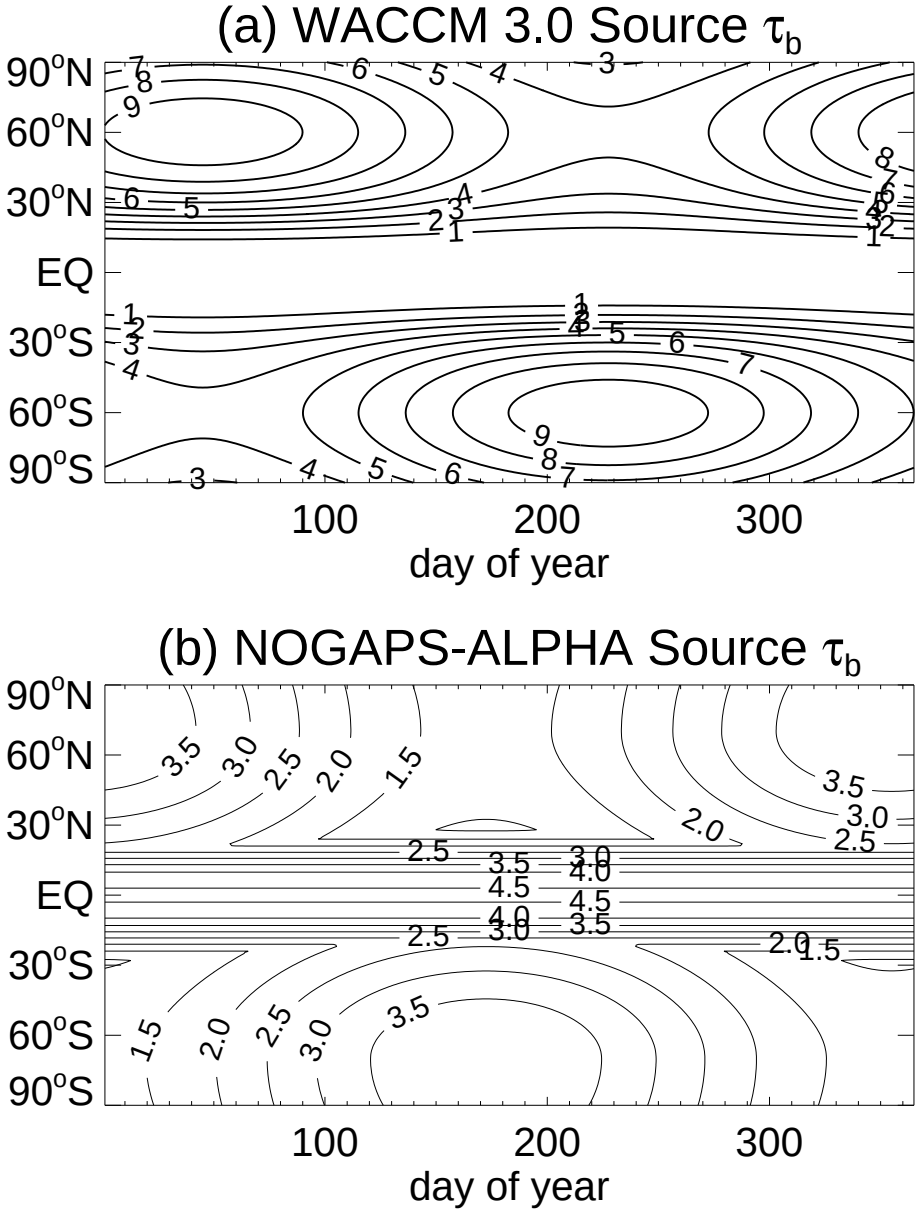

FIG. 1. Background momentum flux τ_b (mPa) based on two different functions $F(\phi, t)$ in (2) used by (a) WACCM 3.0 ($\tau_b^* = 7$ mPa) and (b) NOGAPS-ALPHA ($\tau_b^* = 10$ mPa).

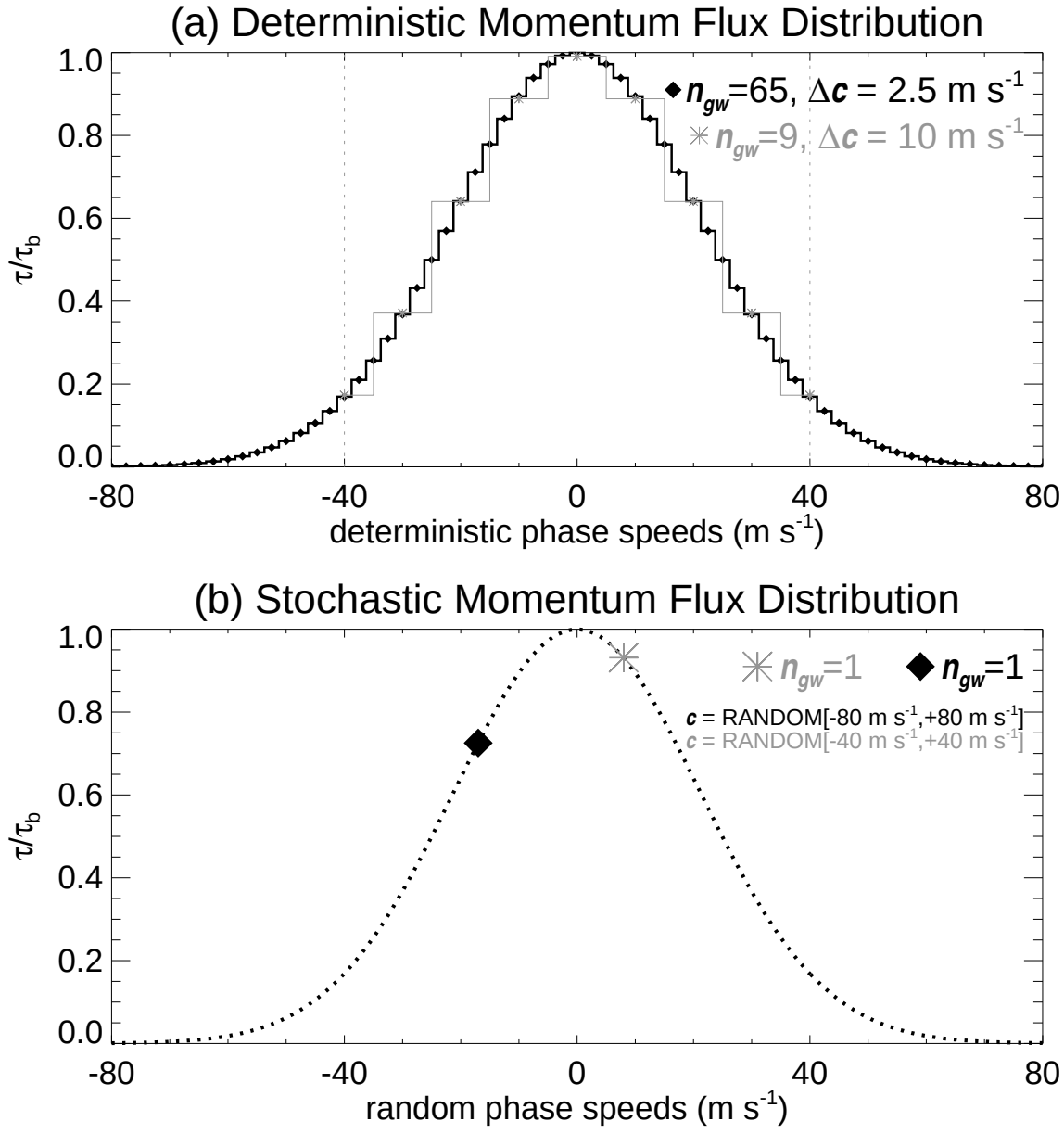

FIG. 2. $\tau_{src}(c_j)/\tau_b$ for (a) $n_{gw} = 65$ discretization of Garcia et al. (2007) and $n_{gw} = 9$ discretization of Kiehl et al. (1996), and (b) the corresponding stochastic analogues.

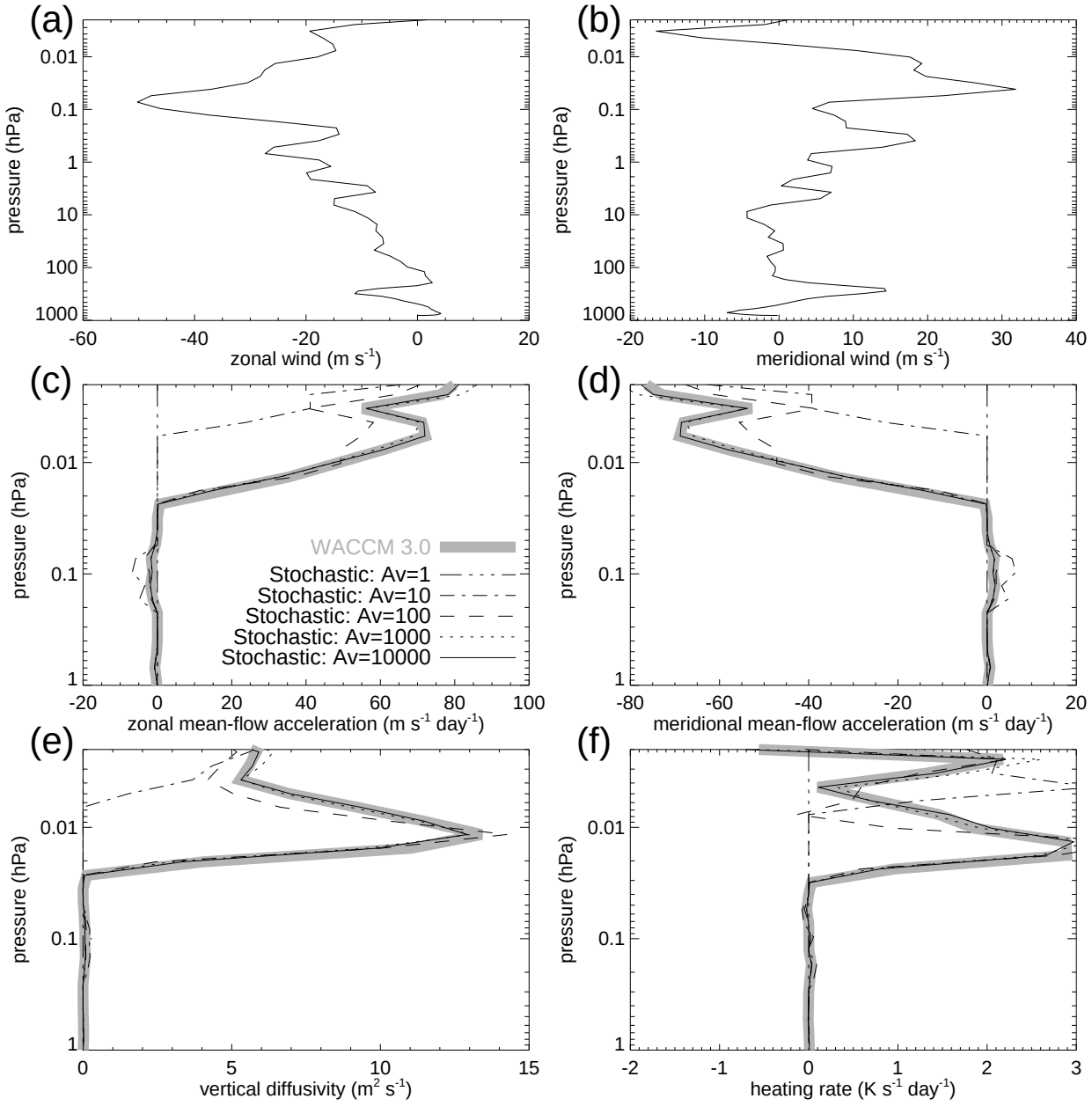

FIG. 3. Vertical profiles of (a) zonal and (b) meridional winds input to gravity wave drag scheme, which returns (c) zonal and (d) meridional mean-flow accelerations, (e) vertical diffusion coefficients, and (f) heating rates. As labeled in panel (c), the gray curves show results from the WACCM 3.0 scheme, while the remaining curves show output from the stochastic analogue averaged over 1, 10, 100, 1000, and 10000 separate calls.

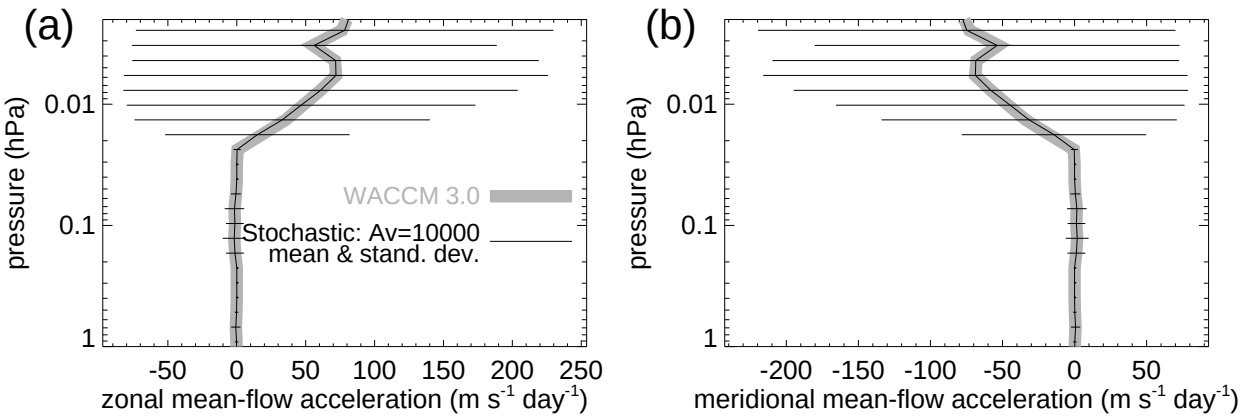

FIG. 4. (a) zonal and (b) meridional mean-flow accelerations from the WACCM 3.0 gravity wave drag scheme (gray curve) and the 10000-point mean from the stochastic analogue (black curve) with corresponding standard deviations shown as error bars.

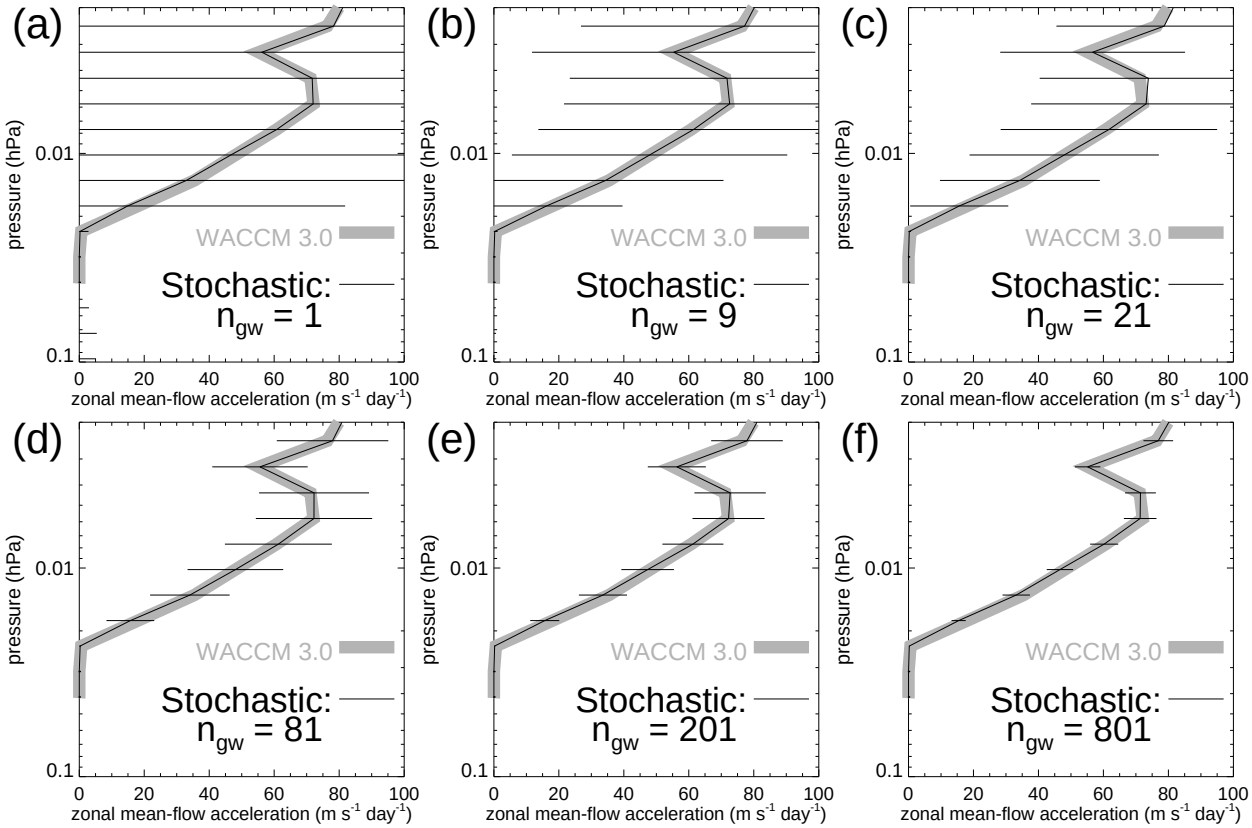

FIG. 5. As in Figure 4a, but now showing means and standard deviations from the stochastic analogue for n_{sgw} values of (a) 1 (same as Figure 4a), (b) 9, (c) 21, (d) 81, (e) 201, and (f) 801. In each case the number of calls was adjusted to yield a total of 10000 waves.

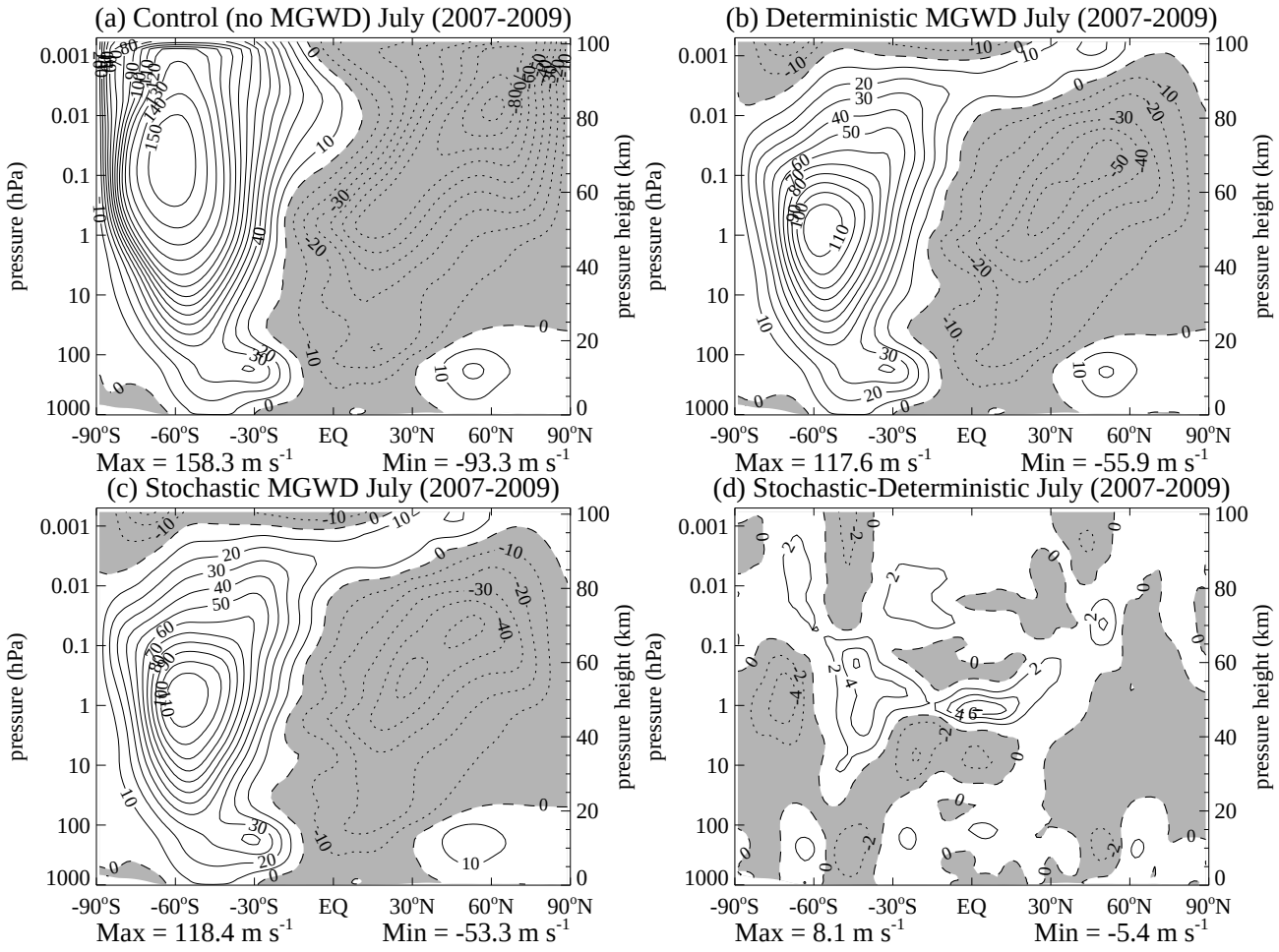

FIG. 6. Zonal-mean zonal winds (m s^{-1}) for July 2007-2009 from NOGAPS-ALPHA nature runs: (a) control run without nonorographic gravity wave drag, and runs using the (b) deterministic and (c) stochastic parameterizations of nonorographic gravity wave drag with equivalent settings to produce the same time-mean drag. Differences in the zonal-mean zonal winds between the stochastic and deterministic simulations are plotted in (d).

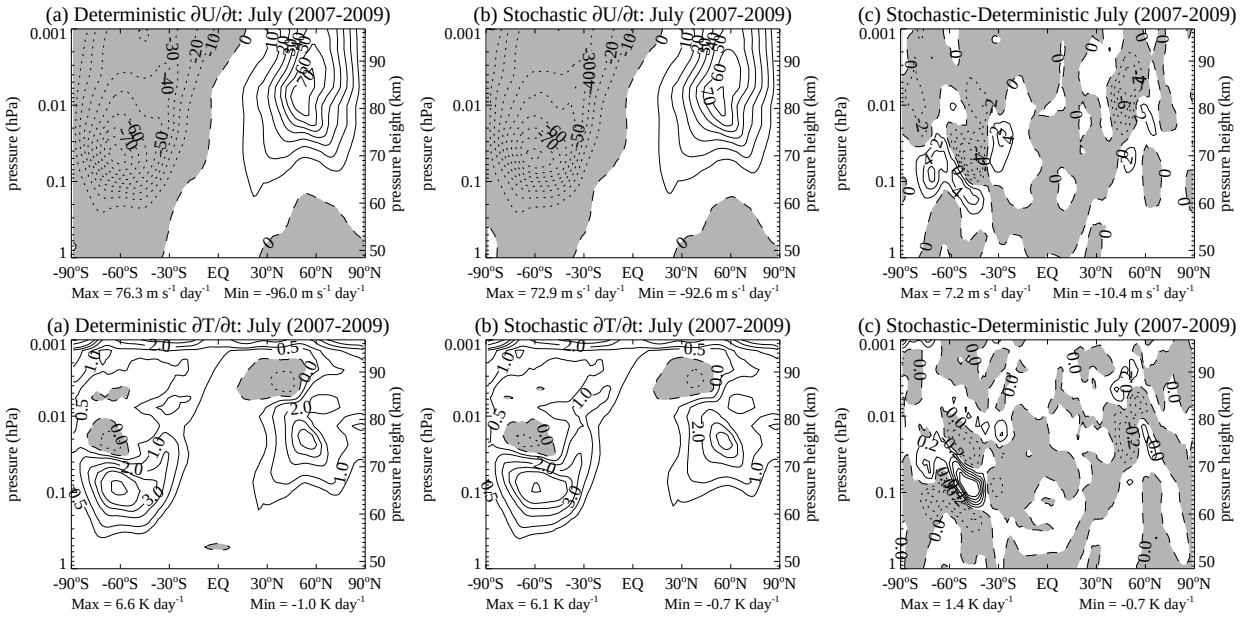

FIG. 7. Zonal-mean zonal mean-flow accelerations (top row, m s^{-1} day^{-1}) and heating rates (bottom row, K day^{-1}) due to parameterized nonorographic gravity wave drag averaged for July 2007-2009 from NOGAPS-ALPHA nature runs using (left column) deterministic and (middle column) stochastic parameterizations. Differences between the two parameterizations are plotted in the right column panels.

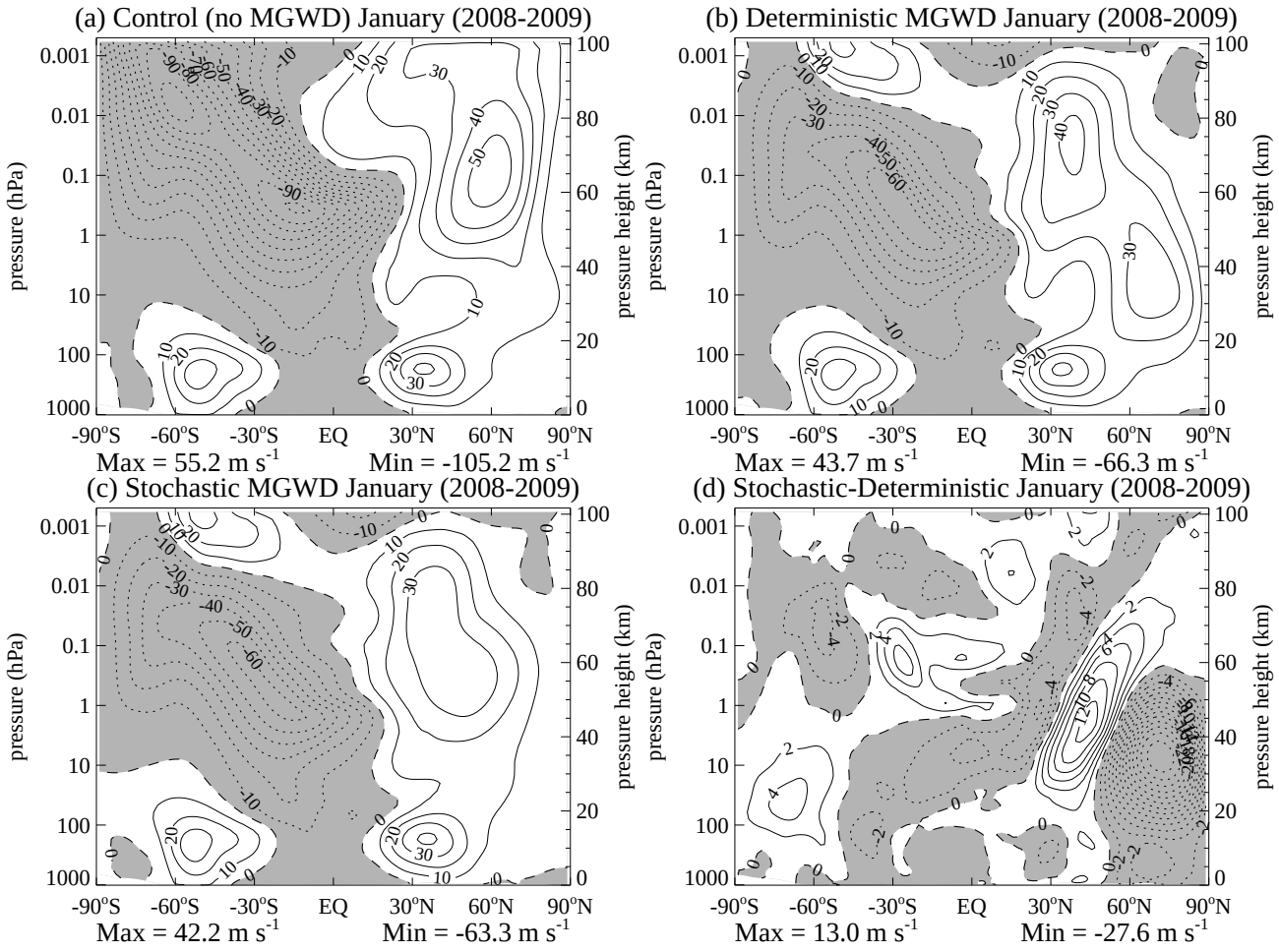

FIG. 8. Zonal-mean zonal winds (m s^{-1}) for January 2008-2009 from NOGAPS-ALPHA nature runs: (a) control run without nonorographic gravity wave drag, and runs using the (b) deterministic and (c) stochastic parameterizations of nonorographic gravity wave drag with equivalent settings to produce the same time-mean drag. Differences in the zonal-mean zonal winds between the stochastic and deterministic simulations are plotted in (d).

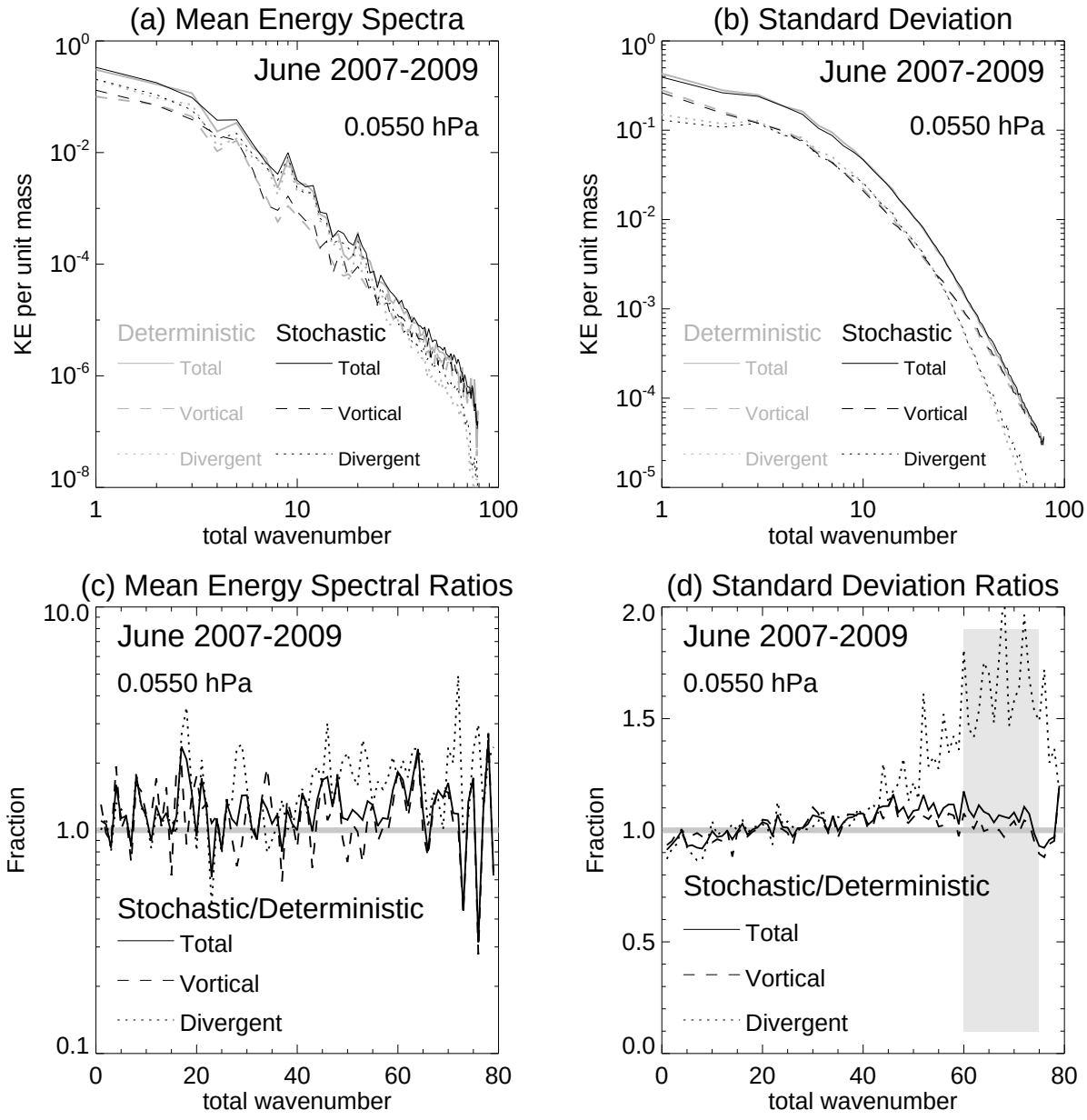

FIG. 9. (a) mean kinetic energy spectra and (b) its standard deviation at each total wavenumber, at 0.055 hPa, averaged from daily 0000 UTC spectral NOGAPS-ALPHA GCM fields for June 2007-2009 for nature runs in which nonorographic gravity-wave drag was parameterized deterministically (gray curves) and stochastically (black curves). The vortical (dashed curves) and divergent (dotted curves) contributions to total kinetic energy (solid curves) are also shown. Panels below show the ratios of the stochastic to the deterministic spectral curves in the panels above. Panel (d) shades the total wavenumber range 60–75 used to form profile means in Figure 10.

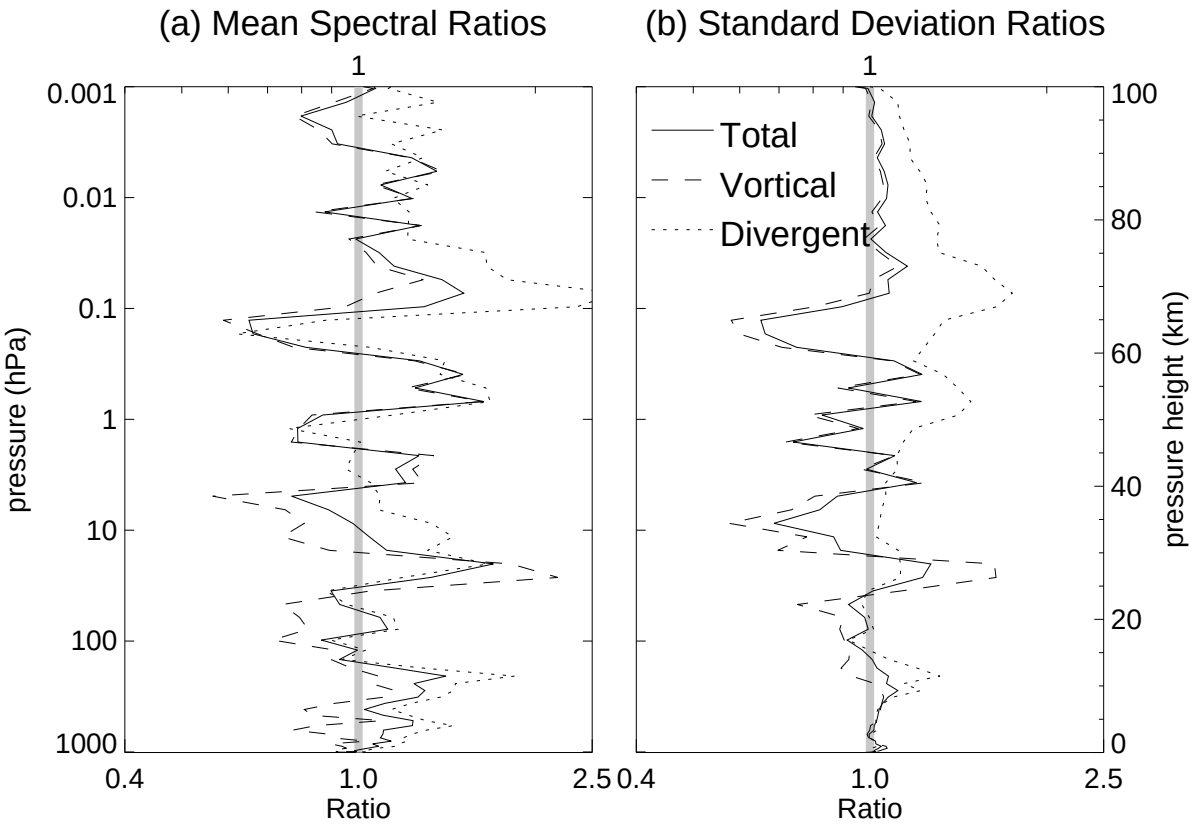

FIG. 10. Ratios of total (solid), divergent (dotted) and vortical (dashed) contributions to (a) mean kinetic energy and (b) its standard deviation in the NOGAPS-ALPHA GCM fields for June 2007–2009 using parameterized stochastic and deterministic nonorographic gravity-wave drag. Each energy value is averaged over the total wavenumber range 60–75, with the resulting ratios between the stochastic and deterministic GCM fields plotted as a function of height. Values greater (less) than unity imply increased (decreased) kinetic energy at wavenumbers 60–75 in the GCM fields with stochastic nonorographic gravity-wave drag, relative to those with deterministic nonorographic gravity-wave drag.